Photochemistry and Photobiology, 2003, 77(5): 550–555

Microanatomical and Biochemical Origins of Normal and Precancerous Cervical Autofluorescence Using Laser-scanning Fluorescence Confocal Microscopy¶

Ina Pavlova[1], Konstantin Sokolov[1], Rebekah Drezek[2], Anais Malpica[3], Michele Follen[4] and Rebecca Richards-Kortum*[1]

[1]Department of Biomedical Engineering, The University of Texas at Austin, Austin, TX;
[2]Department of Bioengineering, Rice University, Houston, TX;
[3]Department of Pathology, University of Texas M.D. Anderson Cancer Center, Houston, TX and
[4]Department of Gynecologic Oncology, University of Texas M.D. Anderson Cancer Center, Houston, TX

Received 6 November 2002; accepted 26 February 2003

ABSTRACT

Clinical studies have shown that *in vivo* fluorescence spectroscopy can improve the diagnosis of cervical precancer. Recent work suggests that epithelial fluorescence increases, whereas stromal fluorescence decreases, with precancer. However, the microanatomic and biochemical sources of fluorescence in living cervical tissue have not yet been established. This study aims to characterize the origins of living normal and precancerous cervical fluorescence at microscopic levels using laser-scanning fluorescence confocal microscopy. Ten pairs of colposcopically normal and abnormal biopsies were obtained; transverse, 200 μm thick, short-term tissue cultures were prepared and imaged when viable with UV (351–364 nm) and 488 nm excitation before and after addition of the vital dye, Mitotracker Orange. In normal epithelium basal epithelial cells showed cytoplasmic fluorescence; parabasal, intermediate and superficial cells showed fluorescence only at the periphery of the cell. In low-grade precancers cytoplasmic fluorescence was visible in the bottom one-third of the epithelium; in high-grade precancers cytoplasmic fluorescence was visible throughout the lower two-thirds of the epithelium. Cytoplasmic fluorescence was colocalized with the MitoTracker probe and is attributed to mitochondrial reduced form of nicotinamide adenine dinucleotide at UV excitation and mitochondrial flavin adenine dinucleotide at 488 nm excitation. Stromal fluorescence originated from matrix fibers; with the development of precancer the density and fluorescence intensity of matrix fibers decrease. Autofluorescence properties of precancerous cervix reflect an increased number of metabolically active mitochondria in epithelial cells and a reduced stromal fluorescence, which can be an indicator for altered communication between precancerous epithelium and stroma. These changes can explain differences in *in vivo* fluorescence spectra of normal and precancerous cervical tissue.

INTRODUCTION

Cervical cancer is the second leading cause of cancer mortality among women worldwide (1). The mortality due to cervical cancer has been reduced enormously because of the successful screening, diagnosis and treatment of this type of cancer. Currently, women are screened using the Papanicolaou (Pap) smear. An abnormal Pap smear is followed by colposcopy, where the cervix is examined using a low-power microscope, and any abnormal areas are biopsied (1). However, current screening and treatment procedures have several important limitations. The Pap smear has a low sensitivity and specificity. Although the sensitivity of colposcopy is high, it lacks specificity, and thus many unnecessary biopsies are performed to confirm a diagnosis of cervical precancer (2). Current screening and detection methods are expensive; over six billion dollars are spent annually in the United States in the detection and treatment of low-grade precancers (3). In the developing world, where more than 80% of cervical cancers occur, adequate resources are not available for screening and detection, and many young women die of a preventable disease.

Optical technologies have the potential to address these limitations and to provide automated, cost-effective tools for detection of cervical precancers (4–16). Diagnostic algorithms based on clinically measured spectra can differentiate normal cervix and precancerous cervix with a high sensitivity and specificity. Because *in vivo* fluorescence can be measured and analyzed in real time using inexpensive, portable and automated instrumentation, it has the potential to decrease the number of unnecessary biopsies, to reduce the level of clinical expertise required and to combine screening, detection and treatment in a single visit. These advantages could address the critical need for cervical cancer screening and detection in the developing world.

The diagnostic ability of fluorescence spectroscopy is believed to be due to its ability to detect biochemical and morphological

¶Posted on the website on 20 March 2003.
*To whom correspondence should be addressed at: Biomedical Engineering Program, ENS 610, Austin, TX 78712, USA. Fax: 512-471-0616; e-mail: kortum@mail.utexas.edu

Abbreviations: AGE, advanced glycation end products; FAD, flavine adenine nucleotide; H&E, hematoxylin and eosin; HGSIL, high-grade squamous intraepithelial lesion; LGSIL, low-grade squamous intraepithelial lesion; MMP, matrix metalloproteinases; NADH, reduced nicotinamide adenine dinucleotide; Pap, Papanicolaou; PBS, phosphate-buffered saline.

changes that occur as normal cervical tissue progresses through the dysplasia to cancer sequence. This progress modifies the metabolic and proliferative rates of epithelial cells, induces angiogenesis and impairs communication between the epithelium and supporting stroma. However, a quantitative understanding of the biological basis for the changes in tissue fluorescence that occur with development of precancer has been difficult to develop for a number of reasons. Cervical tissue is turbid, and scattering and reabsorption of fluorescence perturb the fluorescence spectrum. The analysis of cervical tissue spectra is further complicated by the multilayered structure of the cervix, which consists of a stratified, squamous epithelium and underlying fibrous stroma containing structural proteins such as collagen and elastin and blood vessels. Cell morphology, differentiation and metabolic rate vary throughout the epithelium; cells at the basal layer are least differentiated and most metabolically active, whereas the degree of differentiation increases and the metabolic rate decreases in the intermediate and superficial regions of the epithelium. Fluorescence excitation–emission matrixes of cervical cancer cell suspensions (17–19) indicate that the metabolic indicators, namely, reduced forms of nicotinamide adenine dinucleotide (NADH) and flavin adenine dinucleotide (FAD), are the main source of cellular fluorescence at 350 and 450 nm excitations, respectively. Analysis of cervical stroma indicates that stromal fluorescence is mainly due to collagen (18). In particular, various collagen cross-links ranging from enzymatically formed cross-links to advanced glycation end products (AGE) are most likely the major fluorescence source in the cervical stroma at 310–400 nm excitation (18,20).

Fluorescence microscopy provides a tool to examine the microanatomic distribution of autofluorescence within normal and precancerous cervix. Because the fluorescence signal from cervical epithelium is metabolically sensitive, it is important to image fluorescence of living cervical tissue. Initial microscopic studies of cervical autofluorescence used frozen–thawed tissue, where oxidation upon thawing can alter the fluorescence properties of the epithelial cells (21). Fluorescence of short-term cultures of normal and precancerous human cervical tissue can be imaged using wide-field fluorescence microscopy, observing living epithelium and stroma directly (17,22). Results from a study of short-term cultures from 31 normal biopsies (17) demonstrated that epithelial fluorescence intensity decreases with age, whereas stromal fluorescence intensity increases with age. Fluorescence patterns of short-term tissue cultures from paired normal and precancerous biopsies from 34 patients (22) showed that as precancer develops, both the epithelial and stromal fluorescence are altered. In particular, the overall epithelial fluorescence intensity at 380 nm excitation increased with precancer. Stromal fluorescence decreased at both 380 and 460 nm excitations when tissue progressed from normal to precancerous.

An important limitation of previous studies using short-term tissue cultures is that when the 200 μm thick fresh tissues are imaged with wide-field microscopy, there is insufficient spatial resolution to observe the microanatomic source of the epithelial and stromal fluorescence. This article examines the autofluorescence properties of short-term cultures from normal and precancerous tissue at high spatial resolution using laser-scanning confocal fluorescence microscopy. The goals of the current study are to resolve the fluorescence signal from individual cells in the basal, intermediate and superficial regions of the epithelium and to qualitatively describe differences in the fluorescence pattern of these cells as precancerous changes take place. A further objective of this study is to compare the distribution of epithelial fluorescence with the distribution of metabolically active mitochondria as assessed with a vital fluorescence dye. The final goal of the current study is to resolve the microscopic origin of the stromal fluorescence and to compare this with the density of structural protein fibers within the stroma.

MATERIALS AND METHODS

Biopsy collection and preparation of fresh tissue slices. Cervical biopsies were collected, with informed consent, from volunteers at the colposcopy clinics at The University of Texas M.D. Anderson Cancer Center and Lyndon B. Johnson Hospital. All the volunteers in the study were either referred for colposcopic examination after an abnormal Pap smear or were to be treated for cervical precancer. Before colposcopic examination 6% acetic acid was applied to the cervix. Four biopsies were obtained from each volunteer. Two of the biopsies were collected for research purposes: one from a colposcopically identified precancerous lesion and another from a normal area on the cervix removed from the transformation zone. Two other biopsies were taken from sites adjacent to the first pair of biopsies and were sent for histopathologic examination. All biopsies were obtained from squamous epithelial sites.

After removal, the research biopsies were placed immediately in a chilled (4°C) culture medium (Dulbecco modified Eagle medium without phenol red). Transverse tissue slices were obtained from each biopsy with a microtome, the Krumdieck tissue slicer (MD 1000-A1, Alabama Research and Development, Munford, AL), designed to cut fresh tissue with minimal damage (23). Before slicing, each biopsy was embedded in 4% agarose, and 200 μm thick slices were cut. It has been shown that fresh tissue slices can be maintained viable in culture up to 20 h (23). In our experiments short-term tissue cultures were imaged within 10 h of biopsy removal. Control experiments showed that fluorescence intensity varied less that 10% when imaged immediately after preparation and up to 5.5 h after preparation. Before imaging, the short-term tissue cultures were washed with phosphate-buffered saline (PBS) and placed on a microscope slide. PBS was added to the slide, and the sample was covered with a #1 coverslip. Spacers, approximately 200 μm thick, were placed between the slide and the coverslip to avoid compression of the tissue.

Confocal microscopy. An inverted Leica (TCS 4D) confocal laser-scanning fluorescence microscope was used to obtain optically sectioned fluorescence images of the samples. The microscope was equipped with an argon ion laser, providing excitation in the 351–364 nm range, and an Ar/Kr laser, used for 488 nm excitation. The average power delivered to the tissue was 31–70 μW for 488 nm excitation and 15–30 μW for the UV (351–364 nm) excitation. All images were acquired with a 40× oil-immersion objective, with a numerical aperture of 0.7 and a working distance of 80 μm. Before fluorescence imaging, an area with a well-defined epithelial layer atop basement membrane and underlying stroma was selected in each slice under bright-field illumination. Optical stacks of each region of interest were obtained initially with UV excitation, followed by 488 nm excitation. Each optical stack included 10–13 optical sections, spaced 2 μm apart for a penetration depth of approximately 20–26 μm. A 405–440-nm band-pass filter collected the fluorescence signal at UV (351–364 nm) excitation, and a 512 nm long-pass filter was used at 488 nm excitation. Integration time for each frame was 30 s at both excitation wavelengths.

A control experiment that investigated the degree of photobleaching in cervical tissue at both UV (351–364 nm) and 488 nm was performed. A region of interest was selected and scanned several times for a total duration of 2 min. Then, the fluorescence intensity of the scanned area was compared with that of an unexposed adjacent region. No photobleaching effects were detected at both excitation wavelengths in either tissue layer.

To ensure that the detected signal was due to autofluorescence and was not associated with incomplete rejection of scattered excitation light, a thin layer of scattering, nonfluorescent silica beads (Bangs Laboratories, Fishers, IN), with a refractive index of 1.475 at 360 nm excitation and a mean diameter of 0.6 μm, was imaged with both UV (351–364 nm) and 488 nm excitation using a 40× objective. No signal was detected from the beads under the same conditions used to image cervical tissue.

Image analysis. Optical stacks of six regions of interest were obtained from each short-term tissue culture. Areas of interest included superficial, intermediate, parabasal and basal epithelium and stroma immediately beneath

and 250–500 μm below the basement membrane. The stacks were qualitatively analyzed, and the overall fluorescence patterns in the different regions were compared. To enhance the observation of tissue fluorescence, contrast stretching and pseudocolor were applied to the confocal images.

Vital staining. In a subset of two short-term tissue cultures, the distribution of actively metabolizing mitochondria was compared with the distribution of autofluorescence throughout the epithelium. MitoTracker Orange CM-H_2TMRos (Molecular Probes, Eugene, OR) is a mitochondrial selective probe, which localizes in actively respiring cells. When the probe is absorbed by vital mitochondria, it is oxidized and converted to a fluorescent species with an excitation maximum of 554 nm. A stock solution of MitoTracker Orange was diluted with growth medium Dulbecco modified Eagle medium (DMEM) to a working concentration of 125 n*M*. Short-term tissue cultures were incubated in the MitoTracker solution for 45 min at room temperature. The samples were washed with PBS for 45 min and then imaged with the laser-scanning confocal microscope at excitation wavelengths of 488 nm to image autofluorescence and 568 nm to image probe fluorescence. A 600–630 nm band-pass filter collected the fluorescence signal at 568 nm excitation. A control experiment of unstained short-term tissue cultures showed no detectable autofluorescence at 568 nm excitation under the same conditions used to image MitoTracker Orange fluorescence.

Histologic staining and diagnosis. After fluorescence imaging, the short-term cultures were fixed in 10% formalin and prepared for H&E analysis. A standard H&E protocol was followed. H&E sections were evaluated by a pathologist with expertise in gynecologic pathology, who provided a final diagnosis of the imaged short-term cultures. Pathology results also were available from the second set of biopsies obtained in the clinic and were used to provide final diagnosis for 9 of the 17 short-term tissue cultures that were damaged by the H&E staining and did not undergo a histopathologic analysis.

RESULTS

A total of 10 patients were enrolled in this study. Short-term tissue cultures were obtained and imaged from paired colposcopically normal and abnormal biopsies from seven patients, and for three patients results were obtained only from colposcopically abnormal biopsies. Colposcopic impression was high-grade squamous intraepithelial lesion (HGSIL) for 7 of the 10 abnormal biopsy sites and low-grade squamous intraepithelial lesion (LGSIL) for the remaining three biopsy sites. Upon histopathologic examination of the short-term cultures using standard criteria, five short-term cultures were classified with HGSIL, six were classified with LGSIL and six were classified as normal. Because of the limited sample size, analysis was performed by grouping data from all tissue cultures into normal, LGSIL and HGSIL groups, not taking into account the age and hormonal status of the patients.

Examination of confocal images indicated two distinct patterns of epithelial cell fluorescence at both UV (351–364 nm) and 488 nm excitation. The first pattern is characterized by cells with brightly fluorescent cytoplasm and dark nuclei. In the second type of epithelial cell fluorescence, the majority of the signal originates from the periphery of cells, with a large portion of the cytoplasm showing no fluorescence. Confocal images of most normal short-term tissue cultures showed that the cytoplasmic fluorescence in normal epithelium is limited to a thin layer (approximately 20 μm) of cells in the basal region of the epithelium. Peripheral cell fluorescence, sometimes accompanied by brightly fluorescent nuclei, was observed in the parabasal, intermediate and superficial regions of normal epithelium. Figure 1 shows representative confocal images of normal superficial and intermediate epithelium (Fig. 1a) and of normal basal and parabasal regions (Fig. 1b) at UV excitation. In this particular short-term culture, cytoplasmic fluorescence originates from a single layer of basal epithelial cells situated next to the basement membrane. Peripheral fluorescence is observed throughout the rest of the epithelium.

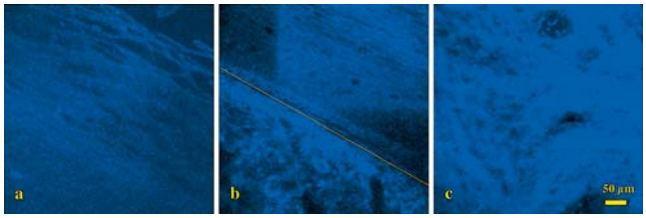

Figure 1. Confocal images of a short-term tissue culture with a normal histopathologic diagnosis. Images were taken with 351–364 nm excitation and a 40× objective: (a) superficial and intermediate epithelium; (b) intermediate, parabasal and basal epithelium with underlying stroma; and (c) stroma approximately 300 μm below the epithelium. The yellow line represents the basement membrane. The biopsy was obtained from a 47 year old patient.

Figure 2 shows confocal images at UV (351–364 nm) excitation from a representative short-term tissue culture with a histopathologic diagnosis of LGSIL. Figure 2a shows fluorescence from the superficial and intermediate epithelial regions. Here the periphery of the epithelial cells exhibits autofluorescence similar to that of normal tissue cultures. Figure 2b shows fluorescence from the parabasal and basal regions of the LGSIL tissue culture; epithelial cells with bright cytoplasmic fluorescence occupy the bottom one-third of the epithelium. Examination of H&E sections prepared from the same LGSIL tissue culture shows that the distribution of cytoplasmic fluorescence corresponds to areas of the epithelium that contain precancer.

Figure 3 shows confocal fluorescence images of a representative tissue culture diagnosed with HGSIL. Here, a larger number of cells with bright cytoplasmic fluorescence are found throughout the upper two-thirds of the epithelium layer, including the superficial and intermediate region (Fig. 3a) and the parabasal and basal regions (Fig. 3a). Figure 3b shows fluorescence of the same sample at 488 nm excitation; the same morphology pattern of fluorescence is seen as in the UV (351–364 nm) excitation image.

Examination of confocal images from stromal regions indicates that stromal fluorescence at both excitation wavelengths is mainly due to fibers forming a compact matrix, which varies in density with stromal depth. UV fluorescence patterns of stroma beneath normal epithelium (Fig. 1b) and stroma approximately 250 μm below the normal epithelium (Fig. 1c) were compared. Collagen fibers from areas adjacent to the normal basement membrane have very bright fluorescence; however, no major differences in the overall fluorescence pattern and matrix density in stromal regions adjacent to and beneath normal epithelial tissue were observed. A fluorescence image at UV (351–364 nm) excitation of the collagen matrix adjacent to LGSIL epithelium is shown in Fig. 2b. The matrix density immediately beneath the LGSIL epithelium was less than the density in normal tissue cultures. In LGSIL samples, matrix density increased with stromal depth, as shown in Fig. 2c. A representative image at UV (351–364 nm) excitation of the stromal fluorescence pattern originating from areas adjacent to the HGSIL epithelium is shown in Fig. 3c. Matrix density is further reduced here, with weak fluorescence intensity beneath the basement membrane. This trend was seen in five out of six HGSIL cases and strongly contrasts with the dense and brightly fluorescent collagen matrix seen in stromal regions that are 250–300 μm below the high-grade dysplastic epithelium (data not shown). A distinct increase in the density and fluorescence intensity of stroma 250–300 μm below the epithelium as compared with stroma beneath the basement membrane was seen in all HGSIL and LGSIL cases.

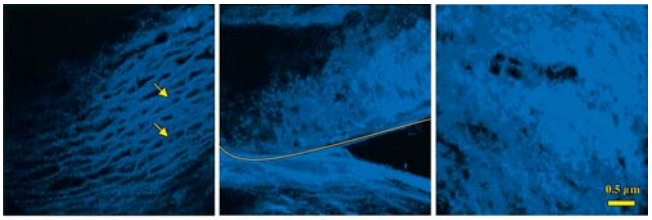

Figure 2. Confocal images of a short-term tissue culture with a histopathologic diagnosis of LGSIL. Images were taken with 351–364 nm excitation and a 40× objective: (a) superficial and intermediate layers of epithelium; (b) intermediate, parabasal and basal layers of epithelium with underlying stroma; and (c) stromal region 250 μm below the epithelium. The yellow line represents the basal membrane, and the arrows indicate nuclear autofluorescence. The biopsy was obtained from a 47 year old patient.

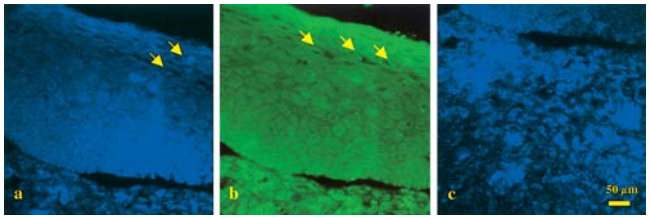

Figure 3. Confocal images of short-term tissue culture with histopathologic diagnosis of HGSIL taken with a 40× objective: (a) epithelium at 351–364 nm excitation; (b) epithelium at 488 nm excitation; and (c) basal layer of epithelium with underlying stroma at 351–364 nm excitation. The biopsy was obtained from a 27 year old patient. The arrows indicate nuclear autofluorescence.

Figure 4 summarizes the observed epithelial and stromal fluorescence patterns and their changes as tissue progresses from normal to precancerous. Normal epithelial fluorescence at UV (351–364 nm) and 488 nm excitation originates from the cytoplasm of basal cells and from the periphery of parabasal, intermediate and superficial cells. With precancerous transformation the number of cells with cytoplasmic fluorescence increases relative to the number of cells with peripheral fluorescence, making the overall epithelium more fluorescent. The stromal fluorescence beneath the basement membrane tends to decrease as the collagen matrix becomes less dense with precancerous transformation.

Bright nuclear fluorescence from cells mostly in the superficial and intermediate region of the epithelium was observed in many of the normal and precancerous tissue cultures (see arrows in Figs. 2a, 3a,b and 4a). Initially, it was believed that this signal might be due to scattered excitation light from the nuclei, which was not rejected by the band-pass or low-pass filters. However, confocal images of highly scattering, nonfluorescent silica beads showed no detectable signal under the same experimental conditions at both excitation wavelengths. Thus, nuclear and peripheral fluorescence signals are most likely not due to incomplete rejection of scattering.

An important objective of this study was to correlate the distribution of metabolically active mitochondria to the distribution of autofluorescence throughout the epithelium. Results from short-term tissue cultures stained with MitoTracker Orange probe demonstrate that there is a cell by cell correspondence between regions with bright MitoTracker probe fluorescence and regions with epithelial cytoplasmic autofluorescence. Figure 5 shows a representative example of a tissue culture stained with MitoTracker probe and imaged with 556 nm (Fig. 5a,c) and 488 nm excitation (Fig. 5b,d). In this tissue slice the epithelial cytoplasmic fluorescence is limited to the basal and parabasal regions of the sample, which correspond to the regions with brightest MitoTracker fluorescence. Weak, diffuse MitoTracker fluorescence is seen in the periphery and the nuclei of intermediate and superficial cells; however, it does not correspond to the dominant, cytoplasmic autofluorescence signal observed in this sample.

DISCUSSION

High-resolution fluorescence imaging of short-term tissue cultures provides a model system to explore the microscopic origins of normal and precancerous cervical autofluorescence. This study demonstrated two distinct patterns of epithelial and stromal fluorescence and showed how these are modulated when precancer develops.

At both UV (351–364 nm) and 488 nm excitation, epithelial fluorescence can be associated with the cytoplasm and periphery of the cell. In normal epithelium, cytoplasmic fluorescence is limited to a thin layer of basal cells. With the development of precancer in the epithelium, the number of cells with cytoplasmic fluorescence increases, occupying the bottom one-third of the epithelium layer in the case of LGSIL and about two-thirds of the whole layer in the case of HGSIL. Moreover, the distribution of cytoplasmic fluorescence correlates directly to that of the mitochondrial vital stain MitoTracker Orange, indicating that cytoplasmic signal is caused by metabolically active mitochondria within epithelial cells, and in particular to mitochondrial NADH fluorescence at UV excitation and FAD fluorescence at 488 nm excitation. Therefore, fluorescence spectroscopy interrogates metabolically active mitochondria within epithelial cells and is sensitive to changes that occur in mitochondrial density distribution within the epithelium as precancer develops in the cervix.

Confocal images of stroma from normal and precancerous short-term tissue cultures indicate that the major source of stromal fluorescence comes from fibers organized in a dense matrix. With the progression from normal tissue to HGSIL, the density of the stromal matrix immediately beneath the epithelium decreased; however, areas that are approximately 250–300 μm beneath the basement membrane did not show a drop in matrix density. Collagen is known to be the main structural protein in the stromal matrix (24), and it has been demonstrated that stromal fluorescence in cervical tissue is caused mainly by collagen cross-links at 310–400 nm excitation (18). Therefore, a decrease in stromal fluorescence is most likely due to decomposition of the collagen fibers, accompanied by a reduction in the concentration of collagen cross-links. It was generally considered that enzymes secreted by tumor cells degrade stromal collagen and the basement membrane to enable microinvasion (25). However, other studies (26,27) point out that the pattern of stromal degradation is more complex and is characterized by induction of matrix metalloproteinase expression in ''host'' stromal cells, activated by altered interaction between precancerous epithelial cell and host stromal cells. Fluorescence spectroscopy probes the collagen matrix density of cervical stroma, which is an important marker for precancerous developments in the cervix.

Epithelial cells, which lack diffuse cytoplasmic fluorescence, show bright peripheral fluorescence accompanied sometimes by fluorescent nuclei. The absence of specific MitoTracker Orange binding to the periphery and nuclei of these epithelial cells indicates that fluorescence from these areas is not caused by meta-

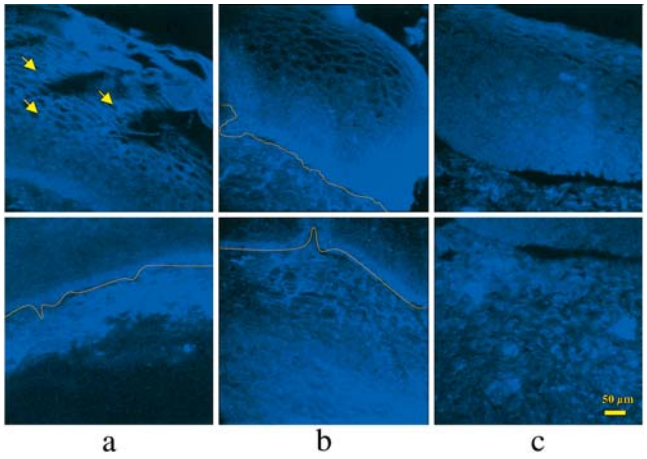

Figure 4. Summary of the trends in epithelial and stromal fluorescence as tissue changes from normal to precancerous: (a) images of epithelium (top) and underlying stroma (bottom) from a normal tissue culture. The weak fluorescence in the bottom part of the stromal image is due to blood absorption. The biopsy was taken from a 22 year old patient; (b) images of LGSIL epithelium (top) and underlying stroma (bottom) taken from the same patient as in (a); and (c) images of HGSIL epithelium (top) and corresponding stroma (bottom) taken from a 27 year old patient. All images were taken at 351–364 nm excitation using a 40× objective. The arrows indicate nuclear autofluorescence.

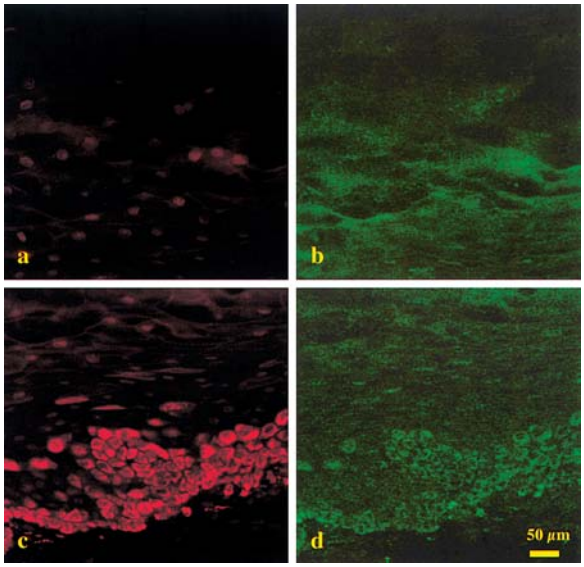

Figure 5. Confocal images of a short-term cervical tissue culture treated with MitoTracker Orange probe. The biopsy was obtained from a 30 year old patient using a 40× objective. The pathological diagnosis was normal, based on the adjacent clinical biopsy and not on the short-term culture directly: (a) superficial and intermediate epithelium at 556 nm excitation showing MitoTracker fluorescence; (b) superficial and intermediate epithelium at 488 nm excitation showing autofluorescence; (c) basal and parabasal epithelium at 556 nm excitation showing MitoTracker fluorescence; and (d) basal and parabasal epithelium at 488 nm excitation showing autofluorescence.

bolically active mitochondria and suggests that it is not due to accumulation of NADH or FAD. On the basis of reviews of keratin expression patterns in precancerous cervical tissue (28) and on studies of the fluorescence properties of keratin fibers extracted from wool (29), it is possible that keratin fluorescence may be responsible for the nuclear and peripheral signal in epithelial cells.

Several systems capable of measuring *in vivo* optical spectra from normal and precancerous cervical sites (7,12,13) or providing fluorescence images of the entire cervix (14,15) can diagnose cervical precancer with a high sensitivity and specificity. Consistently, the fluorescence intensity of precancerous tissue is lower than that of normal tissue, and the peak emission is shifted to a longer wavelength when fluorescence is excited in the UV (337–380 nm) range (7,12,13,16). Georgakoudi and colleagues used a photon-migration model to extract the intrinsic fluorescence spectra from measured tissue fluorescence and reflectance spectra (7,30). Assuming that tissue is homogenous, they fit the intrinsic fluorescence to a linear combination of fluorescence from NADH and collagen. In a pilot study of 35 patients, they found that NADH fluorescence increases on average approximately by a factor of 2 and that collagen fluorescence decreases on average approximately by a factor of 5 as tissue progressed from normal to precancerous (30). These changes are consistent with those observed in this study. However, cervical tissue has a layered structure, with very different optical properties in the stroma and the epithelium. Drezek and colleagues developed a two-layer Monte Carlo–based model and compared measured and predicted tissue spectra (31). For a group of patients with a mean age of 38 years, she found that the fraction of detected fluorescence attributable to epithelial NADH ranged from 18 to 28% in normal tissue and increased to 28–42% in dysplastic tissue, whereas the fraction attributed to stromal collagen was 72–82% in normal tissue and 58–72% in dysplastic tissue. Again these are consistent with the measurements reported here.

However, the results presented here indicate that even within the epithelium the fluorescence properties vary with epithelial depth. Similarly, the fluorescence properties of the stroma differ immediately under a precancerous lesion and 250–500 μm beneath the basement membrane. These changes are dramatic and should be included when developing models of tissue fluorescence.

Further, the data presented here suggest that fiber probe or imaging system design could be optimized to selectively detect the fluorescence changes throughout layers of the epithelium and stroma. For example, Pogue (32) and Pfefer (33) have recently presented Monte Carlo models of fiber probe design to measure tissue fluorescence emphasizing signal from different tissue regions. Ramanujam (34) described a varying aperture-imaging method to profile the depth dependence of fluorescence. The fluorescence micrographs here provide key information, which can be used not only to interpret clinically acquired data but also to design fiber and imaging systems for improved discriminative ability.

Acknowledgements—We acknowledge the contribution of Tatiana Alexenko, Judy Sandela, Alma Sbach, Karen Rabel, John Wright and John Mendelhall in the collection and preparation of specimens and their assistance in data imaging. Financial support from the National Cancer Institute (PO1-CA82710) is gratefully acknowledged.

REFERENCES

1. National Institutes of Health Consensus Development Statement Online (1996). http://consensus.nih.gov/cons/102/102_statement.htm.
2. Mitchell Follen, M., D. Schottenfeld, G. Tortolero-Luna, S. B. Cantor and R. Richards-Kortum (1998) Colposcopy for the diagnosis of squamous intraepithelial lesions. *Obstet. Gynecol.* **91**, 626–631.
3. Kurman, R. J., D. E. Henson, A. L. Herbst, K. L. Noller and M. H. Schiffman (1994) Interim guidelines for management of abnormal cervical cytology. *J. Am. Med. Assoc.* **271**, 1866–1869.

4. Richards-Kortum, R. and E. Sevick-Muraca (1996) Quantitative optical spectroscopy for tissue diagnosis. *Annu. Rev. Phys. Chem.* **47**, 555–606.
5. Wagnieres, G. A., W. M. Star and B. C. Wilson (1998) *In vivo* fluorescence spectroscopy and imaging for oncological applications. *Photochem. Photobiol.* **68**, 603–632.
6. Ramanujam, N. (2000) Fluorescent spectroscopy of neoplastic and non-neoplastic tissues. *Neoplasia* **2**, 89–117.
7. Georgakoudi, I., E. E. Sheets, M. G. Muller, V. Backman, C. P. Crum, K. Badizdegan, R. R. Dasari and M. S. Feld (2002) Trimodal spectroscopy for the detection and characterization of cervical precancers in vivo. *Am. J. Obstet. Gynecol.* **186**, 374–382.
8. Pogue, B. W., M. Mycek and D. Harper (2000) Image analysis for discrimination of cervical neoplasia. *J. Biomed. Opt.* **5**, 72–82.
9. Balas, C. (2001) A novel optical imaging method for the early detection, quantitative grading, and mapping of cancerous and precancerous lesions of cervix. *IEEE T. Biomed. Eng.* **48**, 96–104.
10. Ramanujam, N., M. M. Follen, A. Mahadevan, S. Thomsen, A. Malpica, T. Wright, N. Atkinson and R. Richards-Kortum (1996) Development of a multivariate statistical algorithm to analyze human cervical tissue fluorescence spectra acquired in vivo. *Lasers Surg. Med.* **19**, 46–62.
11. Ramanujam, N., M. M. Follen, A. Mahadevan, S. Thomsen, A. Malpica, T. Wright, N. Atkinson and R. Richards-Kortum (1996) Spectroscopic diagnosis of cervical intraepithelial neoplasia (CIN) *in vivo* using laser induced fluorescence spectra at multiple excitation wavelengths. *Lasers Surg. Med.* **19**, 63–74.
12. Ramanujam, N., M. M. Follen, A. Mahadevan-Jansen, S. L. Thomsen, G. Staerkel, A. Malpica, T. Wright, N. Atkinson and R. Richards-Kortum (1996) Cervical pre-cancer detection using a multivariate statistical algorithm based on laser induced fluorescence spectra at multiple excitation wavelengths. *Photochem. Photobiol.* **6**, 720–735.
13. Nordstrom, R. J., L. Burke, J. M. Niloff and J. F. Myrtle (2001) Identification of cervical intraepithelial neoplasia (CIN) using UV-excited fluorescence and diffuse-reflectance tissue spectroscopy. *Lasers Surg. Med.* **29**, 118–127.
14. Dattamajumdar, A. K., D. Wells, J. Parnell, J. T. Lewis, D. Ganguly and T. C. Wright Jr. (2001) Preliminary experimental results from multicenter clinical trials for detection of cervical precancerous lesions using the Cerviscan system: a novel full-field evoked tissue fluorescence based imaging instruments. 23rd Annual Meeting of IEEE Engineering in Medicine and Biology, Istanbul, Turkey.
15. Ferris, D. G., R. A. Lawhead, E. D. Dickman, N. Holtzapple, J. A. Miller, S. Grogan, S. Bambot, A. Agrawal and M. L. Faupel (2001) Multimodal hyperspectral imaging for the noninvasive diagnosis of cervical neoplasia. *J. Lower Genital Tract Dis.* **5**, 65–72.
16. Weingandt, H., H. Stepp, R. Baumgartner, J. Diebold, W. Xiang and P. Hillemanns (2002) Autofluorescence spectroscopy for the diagnosis of cervical intraepithelial neoplasia. *Ann. Int. J. Obstet. Gynecol.* **109**, 947–951.
17. Brookner, C., M. Follen, I. Boiko, J. Galvan, S. Thomsen, A. Malpica, S. Suzuki, R. Lotan and R. Richards-Kortum (2000) Tissue slices autofluorescence patterns in fresh cervical tissue. *Photochem. Photobiol.* **71**, 730–736.
18. Sokolov, K., J. Galvan, A. Myakov, A. Lacy, R. Lotan and R. Richards-Kortum (2002) Realistic three-dimensional epithelial tissue phantoms for biomedical optics. *J. Biomed. Opt.* **7**, 148–156.
19. Pitts, J. D., R. D. Sloboda, K. H. Dragnev, E. Dmitrovsky and M. Mycek (2001) Autofluorescence characteristics of immortalized and carcinogen-transformed human bronchial epithelial cells. *J. Biomed. Opt.* **6**, 31–40.
20. Bailey, A. J., R. G. Paul and L. Knott (1998) Mechanisms of maturation and ageing of collagen. *Mech. Ageing Dev.* **106**, 1–56.
21. Lohmann, W., J. Mussman, C. Lohmann and W. Kunzel (1989) Native fluorescence of unstained cryo-sections of the cervix uteri compared with histological observation. *Naturwissenschaften.* **96**, 125–127.
22. Drezek, R., C. Brookner, I. Pavlova, I. Boiko, A. Malpica, R. Lotan, M. Follen and R. Richards-Kortum (2001) Autofluorescence microscopy of fresh cervical tissue sections reveals alterations in tissue biochemistry with dysplasia. *Photochem. Photobiol.* **73**, 636–641.
23. Krumdieck, C. L., J. Ernesto Dos Santos and K. Ho (1980) A new instrument for the rapid preparation of tissue slices. *Anal. Biochem.* **104**, 118–123.
24. Kucharz, E. J. (1992) *The Collagens: Biochemistry and Pathophysiology.* Springer-Verlag, Berlin, Germany.
25. Parks, W. C. (1998) *Matrix Metalloproteinases.*Academic Press, San Diego.
26. Heppner, K. J., L. M. Matrisian, R. A. Jensen and W. H. Rodgers (1996) Expression of most matrix metalloproteinase family members in breast cancer represents a tumor-induced host response. *Am. J. Pathol.* **149**, 666–672.
27. Ki Hong, W. and M. Sporn (1997) Recent advances in chemoprevention of cancer. *Science* **278**, 1073–1077.
28. Smedts, F., F. Ramaekers, R. E. Leube, K. Keijser, M. Link and P. Vooijs (1993) Expression of keratins 1,6,15,16, and 20 in normal cervical epithelium, squamous metaplasia, cervical intraepithelial neoplasia, and cervical carcinoma. *Am. J. Pathol.* **142**, 403–412.
29. Smith, G. J. and W. H. Melhuish (1985) Fluorescence and phosphorescence of wool keratin excited by UV-A radiation. *Text. Res. J.* **55**, 304–307.
30. Georgakoudi, I., B. C. Jacobson, M. G. Muller, E. E. Sheets, D. Badizadegan, D. L. Carr-Locke, C. P. Crum, C. W. Boone, R. R. Dasari, J. Van Dam and M. S. Feld (2002) NADH and collagen as in vivo quantitative fluorescent biomarkers of epithelial precancerous changes. *Cancer Res.* **62**, 682–687.
31. Drezek, R., K. Sokolov, U. Utzinger, I. Boiko, A. Malpica, M. Follen and R. Richards-Kortum (2001) Understanding the contributions of NADH and collagen to cervical tissue fluorescence spectra: modeling, measurements, and implications. *J. Biomed. Opt.* **6**, 385–396.
32. Pouge, B. W. and G. Burke (1998) Fiber optic bundle design for quantitative fluorescence measurement from human tissue. *Appl. Opt.* **37**, 7429–7436.
33. Pfefer, J. T., K. T. Schomacker, M. N. Ediger and N. S. Nishioka (2002) Multiple-fiber probe design for fluorescence spectroscopy in tissue. *Appl. Opt.* **41**, 4712–4721.
34. Ramanujam, N. and L. Quan (2002) Relationship between depth of a target in a turbid medium and fluorescence measured by a variable-aperture method. *Opt. Lett.* **27**, 104–106.